Stability Analysis and Control of Nonlinear Behavior in V^2 Switching Buck Converter

Wei Hu[*], Fangying Zhang[†], Xiaoli Long[*], Xinbing Chen[*], and Wenting Deng[*]

[*†]Lab Center, Guangzhou University, Guangzhou, China

Abstract

Mismatch between switching frequency and circuit parameters often occurs in industrial applications, which would lead to instability phenomena. The bifurcation behavior of V^2 controlled buck converter is investigated as the pulse width modulation period is varied. Nonlinear behavior is analyzed based on the monodromy matrix of the system. We observed that the stable period-1 orbit was first transformed to the period-2 bifurcation, which subsequently changed to chaos. The mechanism of the series of period-2 bifurcations shows that the characteristic eigenvalue of the monodromy matrix passes through the unit circle along the negative real axis. Resonant parametric perturbation technique has been applied to prevent the onset of instability. Meanwhile, the extended stability region of the converter is obtained. Simulation and experimental prototypes are built, and the corresponding results verify the theoretical analysis.

I. INTRODUCTION

The V^2 controlled buck converter has been extensively used because of its advantages of rapid load transient response and easy implementation [1]-[4]. The exact small signal model of the system and the design guidelines have been presented in [5]. The mathematical model of the compensated V^2 controlled buck converter has been derived in [6], which verified the stability characteristics of the regulator. A quasi-V^2 adaptive on-time controller for the buck converter has been proposed in [7], which can provide stable operation with small equivalent series resistance of the output capacitor. With the addition of an inductor current ramp estimator, an enhanced V^2-type constant on-time controller, which is used to manipulate the buck converter, has been proposed in [8] to suppress unstable behavior. However, the abovementioned studies mainly focus on technology improvements instead of nonlinear dynamics analysis.

Power regulators are inherently nonlinear circuits with extensive instability phenomena. Therefore, a range of bifurcation behaviors have been observed, such as flip bifurcation [9], Hopf bifurcation [10], border collision [11], quasi-periodicity [12], and chaos [13].

In [14], the authors reported that subharmonic oscillations occur if the duty cycle is greater than 0.5. Slope compensation technology is applied to solve the problem. The describing function model of the V^2 constant on-time controlled buck converter was built in [1]. The subharmonic oscillation point is also predicted successfully. The averaged model based on the Krylov–Bogoliubov–Mitropolsky ripple estimation technique was built in [15], and ripple oscillation instability is solved based on the presented fixed compensation ramp method. In [16], the subharmonic oscillations of V^2 and V^2I_C controlled buck converters were analyzed as the varied output voltages resulted in the alteration of the duty cycle. In [17], the authors studied the instability characteristics of the converter based on the Floquet method as the feedback factor varied and stabilized the entire system with the application of sinusoidal compensation.

However, none of the abovementioned works investigated the mechanism of bifurcation and chaos of the system as the switching frequency varies. Typically, along with variation in the switching frequency, the dynamics of the converter show a series of bifurcations. Thus, whether the object will exhibit a similar phenomenon is still unknown.

Generally speaking, instability phenomena, such as bifurcation, subharmonic oscillation, and intermittent oscillation, are detrimental to industrial electronics. Efforts

have been made to suppress unstable behavior in electronic circuits. Control of chaos was first conceived in [18] by injecting temporal parameter perturbations into the system to force the trajectory to approach the preset stable periodic orbit. A newly developed sliding mode controller with a time-varying manifold dynamic to compensate for the external excitation in chaotic systems was proposed in [19]. The resonant parametric perturbation methods in [20] and [21] have been applied to control chaos in power converters. In [22], a conventional feedback controller was designed to drive the chaotic Duffing equation to one of its inherent multiperiodic orbits. The features of these methods involve the use of an extra state feedback or parameter disturbance to force the unstable periodic orbit back to the stable period-1 limit cycle.

Undoubtedly, instability phenomena exist in the buck converter under V^2 manipulation. The extensive application of these circuits enables people to have a deep understanding of the essence of the phenomenon. Such knowledge could be used to improve the performance of these circuits as well as determine new fields of applications. In this study, the existence of bifurcation and chaos is described by calculating the monodromy matrix of the entire switching period. The mechanism of bifurcation and chaos control is described as well as the extended stable region of the stabilized system.

The paper is organized as follows: The mathematical model of the V^2 controlled buck regulator is described in Section II. The derived monodromy matrix of the closed-loop converter is analyzed in Section III. The mechanism of period-2 bifurcation and chaos exhibited by the system is investigated in Section IV. In Section V, the resonant parametric perturbation technique is applied to suppress the instability. The simulation and experimental results for the verification are given in Section VI, and conclusions are drawn in Section VII.

II.   MATHEMATICAL MODEL OF THE CONVERTER

The circuit diagram of the V^2 controlled buck converter is shown in Fig. 1(a), and steady-state waveforms for the continuous conduction mode are shown in Fig. 1(b), where U_r, R_E, and G_1 are the reference voltage, Equivalent Series Resistance (ESR) of the output capacitor, and feedback amplification factor, respectively. Given that the capacitance is large, voltage u_C is essentially constant, and the output voltage is expressed as follows:

$$u_O = \Delta i_L R_E + u_C. \tag{1}$$

The mathematical model of the V^2 switching technique can be expressed as follows:

$$u_O - U_A = 0. \tag{2}$$
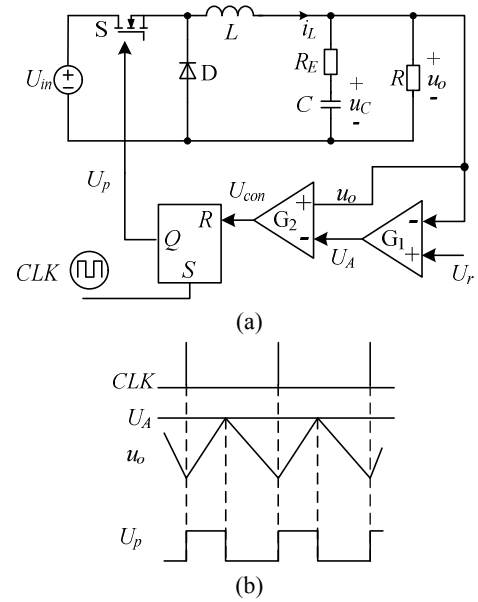
Substituting Eq. (2) and

Fig. 1. V^2 controlled buck converter. (a) Schematic circuit diagram of the system. (b) Illustrated steady-state waveforms.
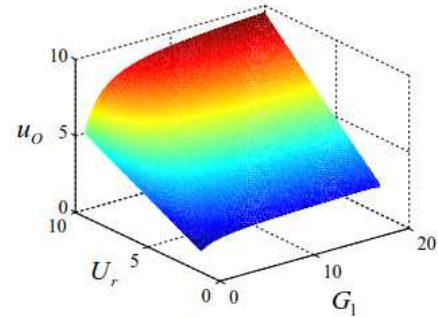

Fig. 2. Relationship of $u_O(U_r, G_1)$

$$U_A = G_1(U_r - u_O) \tag{3}$$

into Eq. (1) obtains

$$u_C - \frac{U_r \cdot G_1}{1 + G_1} + \Delta i_L R_E = 0 \tag{4}$$

and

$$u_O - \frac{U_r \cdot G_1}{1 + G_1} = 0. \tag{5}$$

The value of R_E is small. Therefore, $G_1 \gg 1$ leads to $u_C \approx u_O \approx U_A$. The relationships between u_O, U_r, and G_1 in Eq. (5) are shown in Fig. 2.

Supposing the system begins a new operating period at the time instant of $t = nT$, the switch turns on and the trajectories of the state variable $\mathbf{x} = [i_L, u_C]^T$ run in subsystem $[\mathbf{A}_1, \mathbf{B}_1]$. When the switch is turned off at $t = nT + dT$, the converter runs in subsystem $[\mathbf{A}_2, \mathbf{B}_2]$. Afterward, the state variable $\mathbf{x}$ crosses the switch-off state and then turns back to $\mathbf{x}(nT)$. At the moment when the switch is turned off, the switching surface h_2 is expressed by Eq. (2). Given that the capacity of C is large, u_C is

TABLE I
SYSTEM MATRICES OF V² CONTROLLED BUCK CONVERTER

State matrices		Output matrices	S	D
$A_1 = \dfrac{1}{(R+R_E)}\begin{bmatrix} -\dfrac{RR_E}{L} & -\dfrac{R}{L} \\ \dfrac{R}{C} & -\dfrac{1}{C} \end{bmatrix}$		$B_1 = \begin{bmatrix} \dfrac{1}{L} \\ 0 \end{bmatrix}$	On	Off
$A_2 = \dfrac{1}{(R+R_E)}\begin{bmatrix} -\dfrac{RR_E}{L} & -\dfrac{R}{L} \\ \dfrac{R}{C} & -\dfrac{1}{C} \end{bmatrix}$		$B_2 = \begin{bmatrix} 0 \\ 0 \end{bmatrix}$	Off	On

TABLE II
CIRCUIT PARAMETERS OF V² CONTROLLED BUCK CONVERTER

Parameters	Values	Parameters	Values
U_{in}	12 V	L	200 μH
G_1	20	C	2,200 μF
d	[0, 1]	U_r	5 V
R_E	0.03 Ω	R	3 Ω
G_2	1		

kept almost constant at the switching frequency. As $i_O = u_O/R \approx u_C/R$, the switching surface, where u_O is considered the controlled object, can be rewritten from Eq. (2) as follows:

$$h_{n2} = u_C - \frac{U_r G_1}{1+G_1} + \left(i_L - \frac{u_C}{R}\right)R_E = 0. \tag{6}$$

The state matrices of the subsystems that belong to the converter are shown in Table I.

The system state vectors can be expressed as follows:

$$\boldsymbol{f}_1 = \boldsymbol{A}_1\boldsymbol{x} + \boldsymbol{B}_1 U_{in} = \begin{bmatrix} -\dfrac{RR_E i_L + Ru_C}{L(R+R_E)} \\ \dfrac{Ri_L - u_C}{C(R+R_E)} \end{bmatrix} + \begin{bmatrix} \dfrac{U_{in}}{L} \\ 0 \end{bmatrix}, \tag{7}$$

$$\boldsymbol{f}_2 = \boldsymbol{A}_2\boldsymbol{x} + \boldsymbol{B}_2 U_{in} = \begin{bmatrix} -\dfrac{RR_E i_L + Ru_C}{L(R+R_E)} \\ \dfrac{Ri_L - u_C}{C(R+R_E)} \end{bmatrix}. \tag{8}$$

With respect to a current conduction mode buck converter, the iterated equation of the switching point can be expressed as follows [23]:

$$e^{A_1 dT}\boldsymbol{x}(nT) + A_1^{-1}\left(e^{A_1 dT} - \boldsymbol{I}\right)\boldsymbol{B}_1 U_{in} - \boldsymbol{x}(nT+dT) = 0,$$
$$e^{A_2 d'T}\boldsymbol{x}(nT+dT) + A_2^{-1}\left[e^{A_2 d'T} - \boldsymbol{I}\right]\boldsymbol{B}_2 U_{in} - \boldsymbol{x}\left[(n+1)T\right] = 0. \tag{9}$$

where d is the duty cycle and $d' = 1 - d$.

Numerically solving the previously presented equations using MATLAB with the Newton–Raphson method, the values of $\boldsymbol{x}$ and duty cycle d can be obtained for the periodic orbit.

III. MONODROMY MATRIX

The state variable trajectory of the closed-loop regulator forms a period-1 limit cycle in the phase space over a complete switching period. Based on theory of monodromy matrix [24], [25], if the Floquet multipliers of the monodromy matrix are all within the unit circle, then the system is stable. If the maximum Floquet multiplier equals 1, then bifurcation occurs; otherwise, it is unstable.

Based on Eq. (6), the normal vector and derivative of h_{n2} with respect to time t are expressed as follows:

$$\boldsymbol{n} = \begin{bmatrix} R_E \\ 1 - R_E/R \end{bmatrix}, \tag{10}$$

$$\Delta h = 0. \tag{11}$$

Substituting Eqs. (7) and (8) into Eq. (10) obtains

$$(\boldsymbol{f}_2 - \boldsymbol{f}_1)\boldsymbol{n}^T = \begin{bmatrix} -\dfrac{R_E U_{in}}{L} & -\dfrac{U_{in}(1-R_E/R)}{L} \\ 0 & 0 \end{bmatrix}, \tag{12}$$

$$\boldsymbol{n}^T\boldsymbol{f}_1 = \begin{bmatrix} R_E & 1-R_E/R \end{bmatrix}\left\{\frac{1}{R+R_E}\begin{bmatrix} -\dfrac{RR_E i_L}{L} - \dfrac{Ru_C}{L} \\ \dfrac{Ri_L}{C} - \dfrac{u_C}{C} \end{bmatrix} + \begin{bmatrix} \dfrac{U_{in}}{L} \\ 0 \end{bmatrix}\right\}. \tag{13}$$

Based on Eqs. (10), (11), (12), and (13), the saltation matrix can be expressed as follows:

$$\boldsymbol{S} = \boldsymbol{I} + \frac{[\boldsymbol{f}_2 - \boldsymbol{f}_1]\boldsymbol{n}^T}{\boldsymbol{n}^T\boldsymbol{f}_1 + \Delta h}. \tag{14}$$

Evidently, the following inequality is true:

$$\boldsymbol{n}^T\boldsymbol{f}_2 \times \boldsymbol{n}^T\boldsymbol{f}_1 > 0. \tag{15}$$

Therefore, only one Filippov solution for the switching surface of the system is obtained [26], and the monodromy matrix over one switching period can be expressed as follows:

$$\boldsymbol{M} = \boldsymbol{S}_2\Phi_{off}\boldsymbol{S}_1\Phi_{on} = \Phi_{off}\boldsymbol{S}_1\Phi_{on}. \tag{16}$$

IV. MECHANISM OF THE NONLINEAR BEHAVIOR

The converter is stable and the maximum Floquet multiplier is less than 1 if the switching frequency f is high. With decreasing f, one of the Floquet multipliers goes beyond the unit circle through the negative real line, which marks the onset of instability through a period-2 bifurcation. If f decreases continuously, then the state trajectory of the system will continue to double until it becomes chaotic.

The selected parameters for the system are shown in Table II. The output voltage $u_O = 4.76$ V was obtained by using Eq. (5). The equilibrium points of subsystems S_1 and S_2 are $E_1(4, 12)$ and $E_2(0, 0)$, respectively. Calculating Eq. (9) obtains the Floquet multipliers of monodromy matrix $\boldsymbol{M}$, whose evolution diagram is shown in Fig. 3. To predict the critical value of the bifurcation point and the type, we assume that the absolute value of the maximum Floquet multiplier is 1, that is,
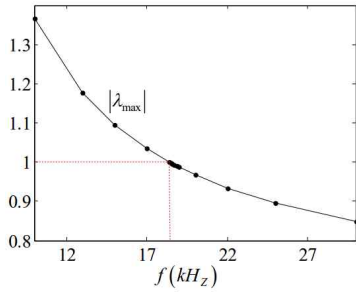
$$\max|\lambda_M| = 1. \tag{17}$$

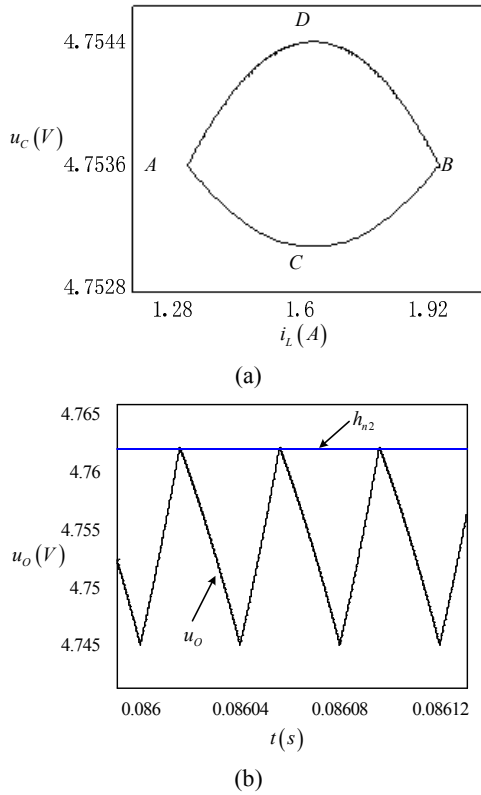Fig. 3. Evolution diagram of the maximum Floquet multiplier.

(a)

(b)

Fig. 4. Stable period-1 waveforms and the switching surface. (a) Phase diagram of i_L–u_O. (b) Output voltage and switching surface.

(a)

(b)

Fig. 5. Period-2 waveforms and the switching surface. (a) Phase diagram of i_L–u_O. (b) Output voltage and switching surface.

Substituting Eq. (16) into Eq. (17) results in f = 18.4 kHz. Thus, the eigenvalues are −1.000 and 0.422, respectively. One of the Floquet multipliers is located at the cross point between the unit circle and the negative real line, which predicts the onset of period-2 bifurcation.

A. Period-1

The closed-loop converter exhibits a periodic steady state at f = 25 kHz, as shown in Fig. 4.

Considering the effect of R_E on the filter capacitor, u_C approximates but is not equal to u_O. The state variable that we selected for use in this study is $x = [i_L, u_C]^T$.

The stable period-1 waveforms are shown in Figs. 4(a) and 4(b). At the beginning of a period, the switch S turns on and the system runs in subsystem S_1 starting from point A. Given
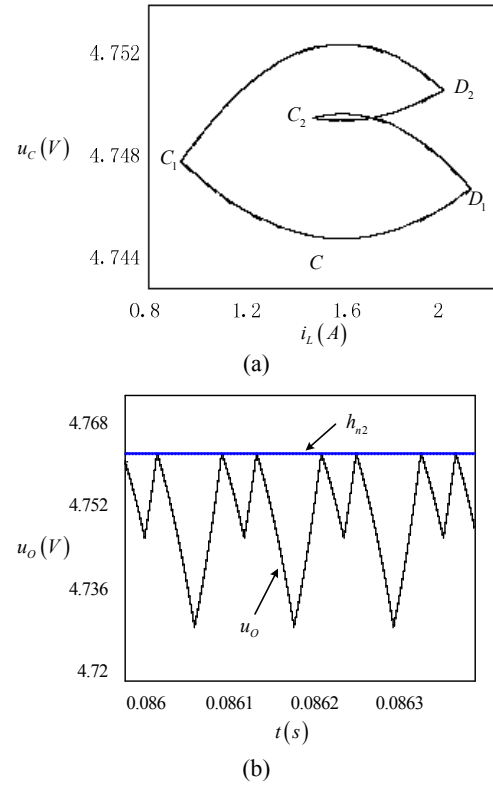
that point A does not locate exactly on the periodic orbit of subsystem S_1, the system will gradually approach the limit cycle that encompasses equilibrium point $E_1(4, 12)$ along the trajectory of ACB, which is the stable periodic orbit of subsystem S_1. After a time interval $t = dT$, the trajectory reaches the switching surface h_2, namely, point B. As a result, the system switches to subsystem S_2 and approaches the equilibrium point $E_2(0, 0)$ starting from point B. The system trajectory is shown as BDA.

B. Period-2 Bifurcation

The period-2 bifurcation of the system with switching frequency at 17 kHz is shown in Fig. 5. Supposing switch tube S turns on at the beginning of the operating period, the converter runs in subsystem S_1 and the starting point is C_1. At this time subinterval, the running trajectory is shown as the curve of C_1–D_1. As soon as the state trajectory reaches the switching surface h_2 at the time instant $t = d_1T$, the switch tube S turns off and the converter switches to subsystem S_2. The running trajectory is shown as the curve of D_1–C_2. At time instant $t = T$, a period is over and the switch S turns on again, with the trajectory approaching C_2 instead of C_1. At this time, the running trajectory is shown as the curve of C_2–D_2. At the time instant $t = T + d_2T$, the state trajectory arrives at the switching surface h_2, the switch turns off, and the converter switches to and runs in subsystem S_2. The running trajectory is shown as the curve of D_2–C_1. When $t = 2T$, the system
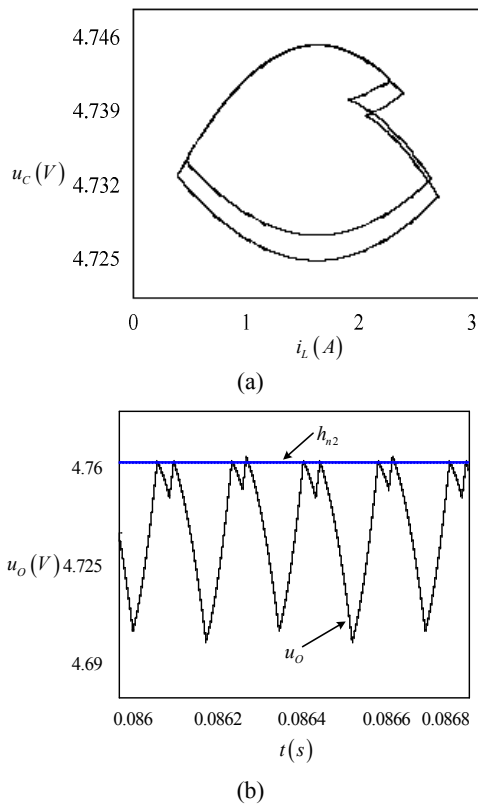
(a)

(b)

Fig. 6. Period-4 waveforms and the switching surface. (a) Phase diagram of i_L–u_O. (b) Output voltage and switching surface.

trajectory goes back to point C_1 and then approaches the next period. Repeating these processes constantly forms the period-2 oscillation.

From the previously discussed analysis, we can conclude that, the steady-state solutions of subsystems S_1 and S_2 remain unchanged when switching frequency f changes. However, with the value of f decreasing, the distance between the switching equilibrium point $x(dT)$ and the switching surface h_2 increases. As a result, the trajectory of subsystem S_1 starting from point C_1 takes a longer time interval, $t = d_1T$, to reach the switching surface h_2 in the first period, which causes the system trajectory to pass point D_1 and reach point C_2 during time $(1 - d_1)T$ when switch S turns off. Then, the second period, starting from point C_2, begins. Consequently, the system trajectory returns to starting point C_1 after two periods $2T$.

C. Period-4 Bifurcation and Chaos

When f = 11.5 kHz, the period-4 bifurcation occurs in the system, as shown in Fig. 6. The mechanism of period-4 bifurcation is similar to period-2 bifurcation and is not discussed here.

As the switching frequency f continues to decrease, period-2 bifurcation correspondingly occurs until chaos is achieved. The phase diagram is shown in Fig. 7, with switching frequency equal to 9.5 kHz and u_C is aperiodic. Many collision points exist between the state trajectory of the system and switching
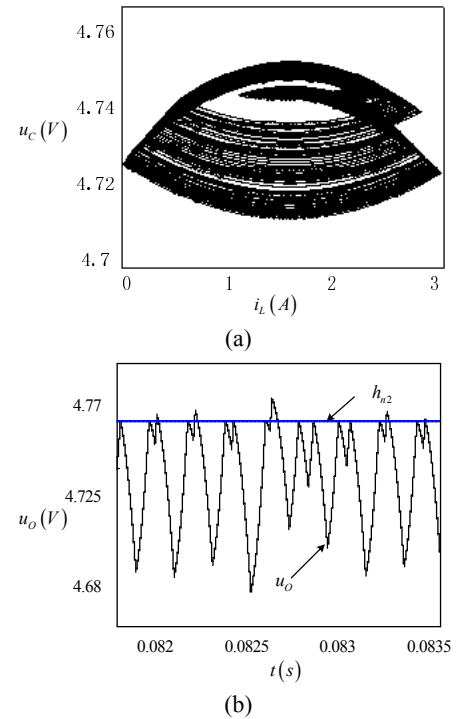

(a)

(b)

Fig. 7. Chaos waveforms and the switching surface. (a) Phase diagram of i_L–u_O. (b) Output voltage and switching surface.

surface h_2. This mechanism can be interpreted as follows: Given that the system trajectory sets off from subsystem S_1, it collides with the switching interface after some time, thereby enabling the system to enter subsystem S_2. Considering the effect of the periodic pulse signal, the system goes back to subsystem S_1. However, the collision points between the state trajectory of the system and switching surface differ with time. As such, if we consider the collision point as the initial value, an infinite number of trajectories run in the subsystem and approach the equilibrium point of S_2 gradually, which generates chaos and oscillation in the system.

V. STABILIZATION CONTROL

The resonant parametric perturbation method is applied to control the aforementioned chaotic system and expand the stability boundary [20]. A sinusoidal signal U_e with the same frequency as driving signal f is added to U_r. The sinusoidal signal U_e takes the form $a\sin(2\pi ft)$. After compensation, the reference voltage can be expressed as follows:

$$U_{re} = U_r + U_e = U_r + a\sin(2\pi ft). \qquad (18)$$

A. Analysis of the Steady-State Error

Adding the reference voltage signal changes the expression of the switching surface h_2 in the system, thereby changing the duty cycle d. The duty cycle of the system before and after sinusoidal voltage compensation is denoted as d and $\tilde{d}$, respectively. The change ratio Δd of the duty cycle is calculated as follows:

f	a_{min}
17.5 kHz	$2.503e^{-4}$
15.5 kHz	$1.455e^{-3}$
12.5 kHz	$1.918e^{-2}$
9.5 kHz	$7.839e^{-2}$
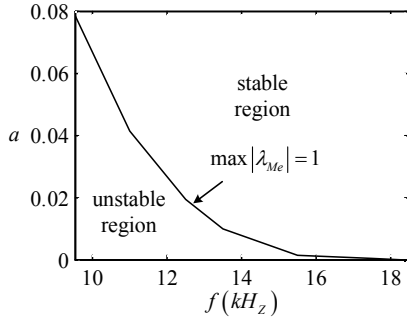
Fig. 8. Region of stability of the period-1 orbit in the a–f parameter space.

$$\Delta d = \frac{(U_{re} - U_r)/U_{in}}{U_r/U_{in}} = \frac{a\sin(2\pi ft)}{U_r} \le \frac{|a|}{U_r}. \quad (19)$$

As the value of a is small, apparently, it could have the possibility $\Delta d \approx 0$. As such, after adding the sinusoidal compensation voltage U_e, the duty cycle of the system, the output voltage, and inductor current hardly vary. Thus, no significant changes were observed for the steady-state error of the system.

B. Monodromy Matrix

With the resonant parametric perturbation added to the system, the switching surface transforms to

$$h_e = u_C - \frac{[U_r + a\sin(2\pi ft)]G_1}{1 + G_1} + \left(i_L - \frac{u_C}{R}\right)R_E = 0. \quad (20)$$

The derivative of the switching surface and the saltation matrix are shown as follows:

$$\Delta h_e = -\frac{2a\pi fG_1\cos(2\pi fd_eT)}{1 + G_1}, \quad (21)$$

$$\boldsymbol{S}_{e1} = \boldsymbol{I} + \left.\frac{(\boldsymbol{f}_{off} - \boldsymbol{f}_{on})\boldsymbol{n}_e^T}{\boldsymbol{n}_e^T\boldsymbol{f}_{on} + \Delta h_e}\right|_{d_eT}, \quad (22)$$
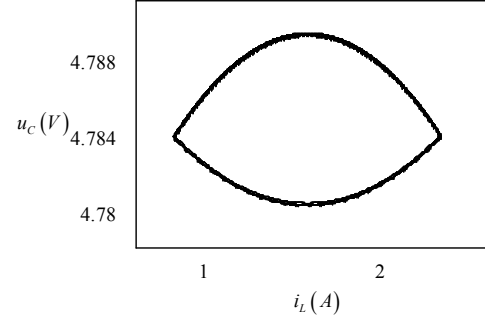
where $\boldsymbol{n}_e = [R_E \quad 1 - R_E/R]^T$.

The transmission matrices are denoted as $\Phi_{eon} = e^{A_1 d_e T}$ and $\Phi_{eoff} = e^{A_2(1-d_e)T}$. The monodromy matrix is expressed as follows:

$$\boldsymbol{M}_e = \Phi_{eoff}\boldsymbol{S}_{e1}\Phi_{eon}. \quad (23)$$
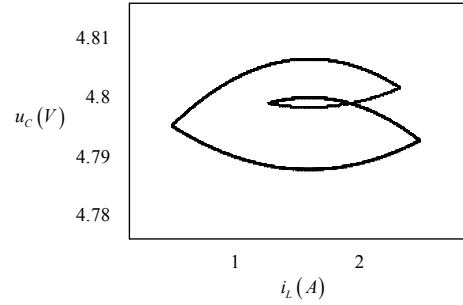
The minimum boundary of a_{min} is shown in Table III and Fig. 8 based on Eq. (23).
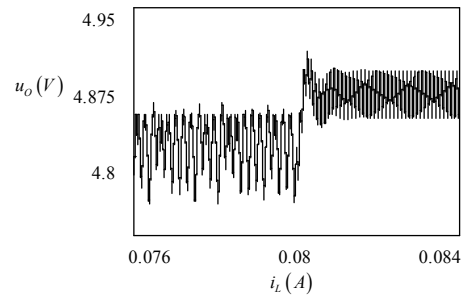
TABLE IV
FLOQUET MULTIPLIER AT $f = 9.5$ kHz

a	λ_{Me}	$Max|\lambda_{Me}|$	State
0.078	−1.0897, 0.1387	1.0897	Period-2 bifurcation
0.08	−0.9907, 0.1208	0.9907	Stable period-1

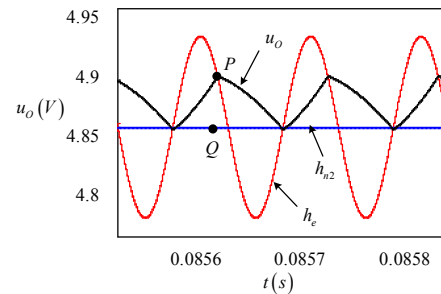

(a)

(b)

Fig. 9. Phase diagram after stabilization control at $f = 9.5$ kHz. (a) Stable period-1 at $a = 0.08$. (b) Period-2 bifurcation at $a = 0.078$.

(a)

(b)

Fig. 10. Waveforms of output voltage. (a) Transient responses of the output voltage. (b) Output voltage u_O and switching surfaces h_e and h_{n2}.
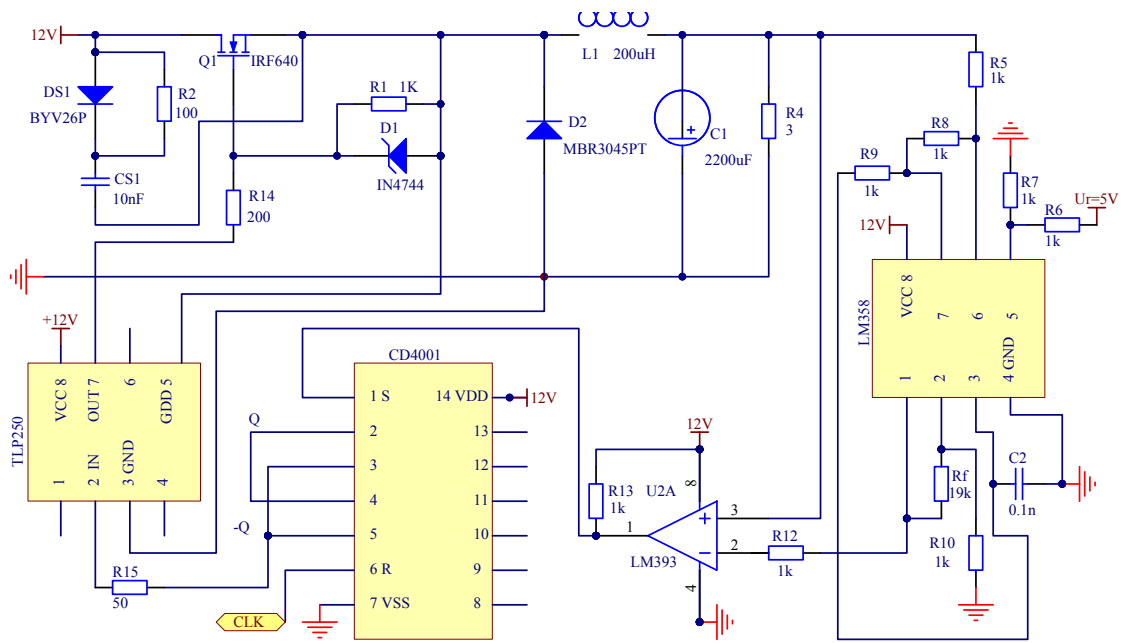
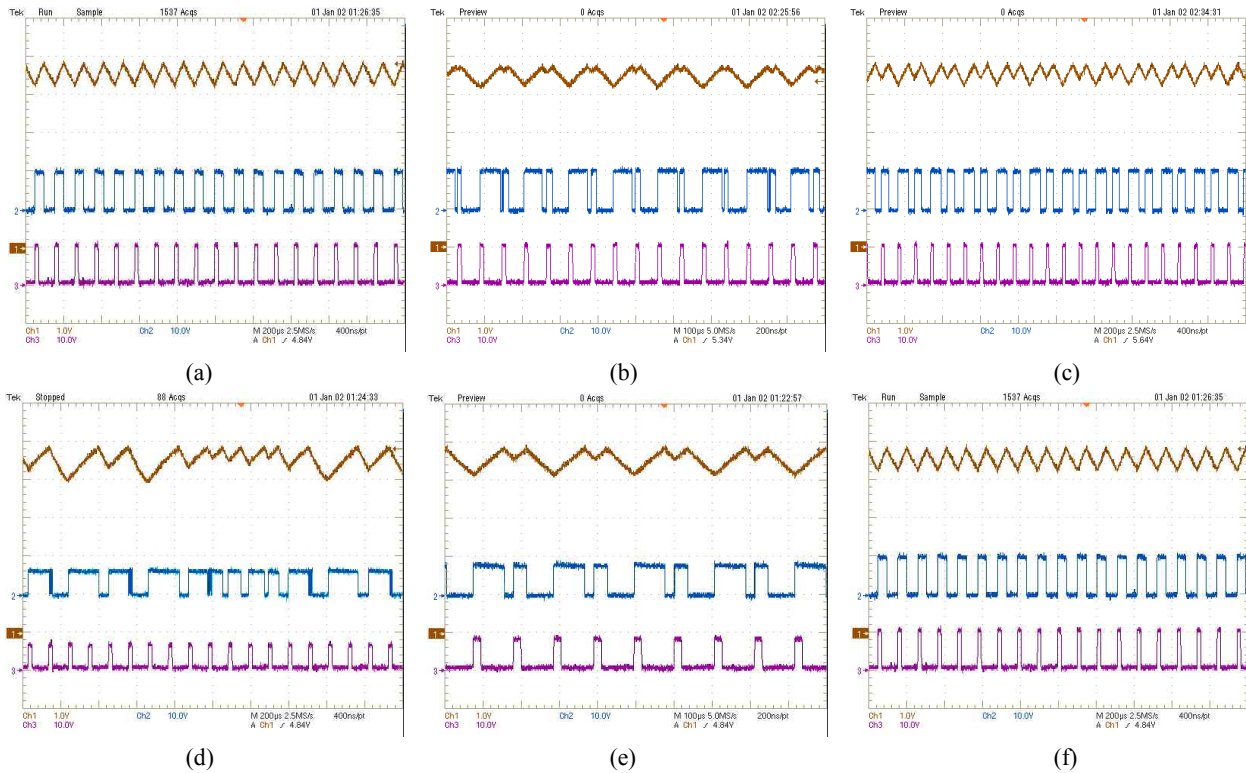Fig. 11. Circuit diagram of V^2 controlled buck converter.

Fig. 12. Experimental waveforms of V^2 controlled buck converter. (a) The waveforms of period-1 when f = 25 kHz. (b) Period-2 bifurcation when f = 17 kHz. (c) Period-4 bifurcation when f = 11.5 kHz. (d) Chaos when f = 9.5 kHz. (e) Controlling chaos to period-2 bifurcation when a = 0.078. (f) Controlling chaos to stable period-1 when a = 0.08.

To verify the stable region shown in Fig. 8, the simulation results around the boundary conditions are given as follows: Based on Fig. 8, the stable boundary at f = 9.5 kHz is a = 0.07839. At the time instant t = 0.08 s, two sinusoidal compensation voltages, U_e = 0.078sin($2\pi ft$) and U_e = 0.08sin($2\pi ft$), are added to U_r. The values of the switching point and characteristic multiplier are shown in Table IV. The phase diagrams of the two simulations are shown in Fig. 9. The system is stabilized to period-2 bifurcation at a = 0.078 and enters the stable period-1 trajectory at a = 0.08. The transient

responses of the output voltage and switching surface are shown in Fig. 10.

C. Mechanism of Chaos Control

Before and after perturbation is applied, the switching surfaces shown in Fig. 9(b) are expressed as follows:

$$h_{n2} = u_C + \left(i_L - \frac{u_C}{R}\right)R_E - \frac{U_r G_1}{1 + G_1} = 0, \quad (24)$$

$$h_e = u_C + \left(i_L - \frac{u_C}{R}\right)R_E - \frac{\left[U_r + a\sin(2\pi ft)\right]G_1}{1 + G_1} = 0. \quad (25)$$

Compensation enables the output voltage of the converter u_O to intersect point P (which belongs to h_e) instead of point Q, which shortens the distance between the equilibrium point $x(d_e T)$ and the switching surface h_2, which decreases the duty cycle of the system. The converter was forced back to stable period-1 orbit.

VI. EXPERIMENTAL DETAILS

The experimental circuit diagram shown in Fig. 11 is set up based on Fig. 1. In the experiment, the IRF640 type MOSFET and MBR3045PT are selected as the power switch and diode, respectively. The pulse signal and the sine compensation voltage signal are generated by a dual output function signal generator. We use LM358 and LM393 as the amplifier and comparator, respectively. The RS flip-flop consists of CD4001, whereas the drive circuit is equipped with the TLP250 and is supplied by an independent +12 power source.

In the converter, the ESR of the output capacitor significantly influences the instability behavior of the regulator. To facilitate integration, the ESR is shown in Fig. 1. However, in industrial application, the ESR will not actually be implemented. As a result, u_C and u_O are equal to each other.

The experimental waveforms of the closed-loop system are shown in Figs. 12(a) to 12(f). After sinusoidal signal compensation, $U_e = 0.078\sin(2\pi ft)$ and $U_e = 0.08\sin(2\pi ft)$ are added to the reference voltage U_r. Then, the system will be stabilized to the period-2 bifurcation or the stable state of period-1. Considering the parasitic parameters and measurement errors, the experiment results slightly deviate from the simulation. In particular, when the compensation voltage $U_e = 0.8\sin(2\pi ft)$ is injected to the system, period-2 bifurcation was achieved instead of the stable state of period-1. By contrast, the system achieves the stable state of period-1 when $U_e = 0.2\sin(2\pi ft)$ is applied to the experiment. However, the state deviation is small and the analytical method is proven to be effective.

VII. CONCLUSIONS

The switching frequency of the converter is an important design objective in the power supply field. An improper switching frequency would render the system unstable, which is often encountered by engineers. A detailed analysis of a buck converter manipulated using the V^2 technique with variations in the operating period is conducted based on the resulting monodromy matrix. The switching frequency taken as the bifurcation parameter reveals some interesting nonlinear phenomena in the converter. With the decrease in f, the series of period-2 bifurcation up to the chaotic state is observed. The mechanism of bifurcation and chaos is analyzed in detail in this study. To suppress the instability behavior, the so-called resonant parametric perturbation technique is applied, which helps control the chaos phenomenon. The extended stable region of the stabilized system is obtained, which is proven to be true by the simulation and experimental results.

REFERENCES

[1] J. Li and F. C. Lee, "Modeling of V^2 Current-Mode Control," *IEEE Trans. Circuits Syst. I, Reg. Papers*, vol. 57, no. 9, pp. 2552-2563, Sept. 2010.

[2] D. Gorder and W. R. Pelletier, "V^2 architecture provides ultra fast transient response in switch mode power supplies," in *Proc. HFPC Conf.*, pp. 19-23, 1996.

[3] D. Gorder, "Switching regulators," U.S. Patent 5 770 940, 1998.

[4] G. H. Zhou, J. P. Xu, and J. P. Wang, "Constant-frequency peak-ripple-based control of buck converter in CCM: review, unification and duality," *IEEE Trans. Ind. Electron.*, Vol. 61, No. 3, pp. 1280-1291, Mar. 2014.

[5] S. Qu, "Modeling and design considerations of V^2 controlled buck regulator," in *Proc. IEEE Apply Power Electron. Conf. Expo.*, pp. 507-513, 2001.

[6] F. Wang, J. Xu, and J. Xu, "Small-signal model of V^2 control technique with compensation," in *Proc. IEEE Int. Conf. Commun. Circuits Syst.*, Vol. 2, pp. 27-29, 2004.

[7] C. Tsai, S.-M. Lin, and C.-S. Huang, "A fast-transient quasi-V^2 switching buck regulator using AOT control with a load current correction (LCC) technique," *IEEE Trans. Power Electron.*, Vol. 28, No. 8, pp. 3949-3957, Aug. 2013.

[8] K. Y. Cheng, F. Yu, F. C. Lee, and P. Mattavelli, "Digital enhanced V^2-type constant on-time control using inductor current ramp estimation for a buck converter with low-ESR capacitors," *IEEE Trans. Power Electron.*, Vol. 28, No. 3, pp. 1241-1252, Mar. 2013.

[9] C. K. Tse, "Flip bifurcation and chaos in three-state boost switching regulators," *IEEE Trans. Circuits Syst. I Fundam. Theory Appl.*, Vol. 41, No. 1, pp. 16-23, Jan. 1994.

[10] A. El Aroudi, L. Benadero, E. Toribio, and G. Olivar, "Hopf bifurcation and chaos from torus breakdown in a PWM voltage-controlled DC-DC boost converter," *IEEE Trans. Circuits Syst. I, Fundam. Theory Appl.*, Vol. 46, No. 11, pp. 1374-1382, Nov. 1999.

[11] S. Maity, "Dynamics and stability issues of a discretized sliding-mode controlled DC-DC buck converter governed by fixed-event-time switching," *IEEE Trans. Circuits Syst. I, Reg. Papers*, Vol. 60, No. 6, pp. 1657-1669, Dec. 2013.

[12] C. C. Fang, "Bifurcation boundary conditions for current programmed PWM DC-DC converters at light loading," *Int. J. Electron.*, Vol. 99, No. 10, pp. 1365-1393, Apr. 2012.

[13] P. Deivasundari, G. Uma, and K. Murali, "Chaotic dynamics of voltage-mode controlled buck converter with periodic interference signals," *Int. J. Bifurcat. Chaos*, Vol. 23, No. 6, Jun. 2013.

[14] G. H. Zhou, J. P. Xu, Y. Y. Jin, and J. Sha, "Stability analysis of V^2 controlled buck converter operating in CCM and DCM," in *Int. Conf. Commun., Circuits. Syst.*, pp. 551-555, 2010.

[15] J. Sun, "Characterization and performance comparison of ripple-based control for voltage regulator modules," *IEEE Trans. Power Electron.*, Vol. 21, No. 2, pp. 346-353, Mar. 2006.

[16] J. Cortés, "Modelling, analysis and optimization of analog controls for a Buck converter," Master Thesis, Universidad Politécnica de Madrid, chap. 3, 2013.

[17] F. Zhang, R. Yang, X. Long, C. Y. Xie, and H. Chen, "Mechanism of instability behaviors and stabilization on V^2 controlled buck converter," *Acta Phys. Sin.*, Vol. 62, No. 21, Dec. 2013.

[18] E. Ott, C. Grebogi, and J. A. Yorke, "Controlling chaos," *Phys. Rev. Lett.*, Vol. 64, No. 11, pp. 1196-1199, Mar. 1990.

[19] C. Fuh and H. Tsai, "Control of discrete-time chaotic systems via feedback linearization," *Chaos Soliton. Fract.*, Vol. 13, pp. 285-294, Feb. 2002.

[20] Y. Zhou, C. K. Tse, S.-S. Qiu, and F. C. M. Lau, "Applying resonant parametric perturbation to control chaos in the buck DC/DC converter with phase shift and frequency mismatch considerations," *Int. J. Bifurcat. Chaos*, Vol. 13, No. 11, pp. 3459-3471, Nov. 2003.

[21] B. Bao, G. Zhou, J. Xu, and Z. Liu, "Unified classification of operation-state regions for switching converters with ramp compensation," *IEEE Trans. Power Electron.*, Vol. 26, No. 7, pp. 1968-1975, Jul. 2011.

[22] G. Chen and X. Dong, "On feedback control of chaotic continuous-time systems," *IEEE Trans. Circuits Syst. I, Fundam. Theory Appl.*, Vol. 40, No. 9, pp. 591-601, Sep. 1993.

[23] S. Samanta, S. Mukhopadhyay, and R. Sheehan, "Discrete-time simulation of a peak current controlled DC/DC buck converter using modal decomposition," *IET Power Electron.*, Vol. 4, No. 6, pp. 642-650, Jul. 2011.

[24] D. Giaouris, S. Banerjee, B. Zahawi, and V. Pickert, "Stability analysis of the continuous-conduction-mode buck converter via Filippov's method," *IEEE Trans. Circuits Syst. I, Reg. Papers*, Vol. 55, No. 4, pp. 1084-1096, May 2008.

[25] R. I. Leine, D. H. Van Campen, and B. L. Van de Vrande, "Bifurcations in nonlinear discontinuous systems," *Nonlinear Dynam.*, Vol. 23, No. 2, pp. 105-164, Oct. 2000.

[26] A. F. Filippov, "Differential equations with discontinuous right-hand side," *American Mathematical Society Translations*, Vol. 42, No. 2, pp. 199-231, 1964.

Wei Hu was born in Ningxiang, China, in 1980. He received his B.S. and M.S. degrees from the College of Electrical and Information Engineering, Hunan University, Changsha, China, in 2003 and 2006, respectively. He is currently working toward a Ph.D. degree. Since 2006, he has been with Guangzhou University, Guangzhou, where he is currently an experimentalist in the Lab Center. His current research interests include modeling and nonlinear control of power converters and stability analysis of DC–DC converters.

Fangying Zhang was born in Hubei, China, in 1981. She received her B.S. degree in Electronics and Information Engineering from Hubei University of Technology, China, in 2003 and her M.S. degree in Geodetic Survey from Wuhan University, Wuhan, China, in 2006. She is currently an experimentalist in the Lab Center at Guangzhou University. Her current research interests include modeling and nonlinear control of power converters and stability analysis of DC–DC converters.

Xiaoli Long was born in Xiangtan, China, in 1966. She received her M.S. degree from South China University of Technology in 2001. Her current research interests include robotic control and stability analysis of DC–DC converters.

Xinbing Chen was born in Henan, China, in 1978. His current research interests include modeling and nonlinear control of power converters and stability analysis of DC–DC converters.

Wenting Deng was born in Hunan, China, in 1983. Her current research interests include modeling and nonlinear control of power converters and stability analysis of DC–DC converters.